# Outbursts Large and Small from EXO 2030+375

Colleen A. Wilson, Mark. H. Finger

VP62, National Space Science and Technology Center, 320 Sparkman Drive, Huntsville, AL 35805

colleen.wilson@nasa.gov

Ascensión Camero Arranz

GACE/ICMUV, Universidad de Valencia, P.O. Box 20085, 46071 Valencia, Spain

### ABSTRACT

During the summer of 2006, the accreting X-ray pulsar EXO 2030+375 underwent its first giant outburst since its discovery in 1985. Our observations include the first ever of the rise of a giant outburst of EXO 2030+375. EXO 2030+375 was monitored daily with the Rossi X-ray Timing Explorer (RXTE) from 2006 June through 2007 May. During the giant outburst, we discovered evidence for a cyclotron feature at  $\sim 11$  keV. This feature was confidently detected for about 90 days, during the brighter portion of the outburst. Daily observations of the next five EXO 2030+375 orbits detected pulsations at all orbital phases and normal outbursts shifted to a later orbital phase than before the giant outburst. An accretion disk appears to be present in both the normal and giant outbursts, suggesting that the long-term behavior is a product of the state of the Be star disk and the accretion disk. Here we will present flux and frequency histories from our detailed RXTE observations of the giant outburst and the normal outbursts that surrounded it. A new orbital analysis is presented that includes observations from 1991 through 2007 August.

Subject headings: accretion—stars:pulsars:individual:(EXO 2030+375)—X-rays: binaries

# 1. Introduction

Be/X-ray binaries are the most common type of accreting X-ray pulsar systems observed. They consist of a pulsar and a Be (or Oe) star, a main sequence star of spectral type B (or O) that shows Balmer emission lines (See e.g., Porter & Rivinus 2003, for a review.) The line emission is believed to be associated with circumstellar material shed by the Be star into its equatorial plane. The exact nature of the mass loss process is unknown, but it is thought to be related to the rapid rotation of the Be star, typically near 70% of the critical break-up velocity (Porter 1996). The equatorial material forms a slow, dense outflow, which is generally believed to fuel the X-ray outbursts. Near the Be star, the equatorial outflow probably forms a quasi-Keplerian disk (Quirrenbach et al. 1997; Hanuschik 1996).

X-ray outbursts are produced when the pulsar interacts with the Be star's disk. Be/X-ray binaries typically show two types of outburst behavior: (a) giant outbursts (or type II), characterized by high luminosities and high spin-up rates (i.e., a significant increase in pulse frequency) and (b) normal outbursts (or type I), characterized by lower luminosities, low spin-up rates (if any), and repeated occurrence at the orbital period (Stella, White, & Rosner 1986; Bildsten et al. 1997). As a population Be/X-ray binaries show a correlation between their spin and orbital periods (Corbet 1986; Waters & van Kerkwijk 1989).

For isolated Be stars, variations in the infrared bands (J,H,K) are believed to be good indicators of the size of the Be star's disk. However, when the Be star is in a binary system with a neutron star, the Be disk is truncated at a resonance radius by tidal forces from the orbit of the neutron star (Okazaki & Negueruela 2001). In these systems, since the disk cannot easily change size because of the truncation radius, changes in mass loss from the Be star produce changes in the disk density, which can even become optically thick at infrared wavelengths (see, e.g., Negueruela et al. 2001; Miroshnichenko et al. 2001).

EXO 2030+375 is a 42-s transient accreting X-ray pulsar discovered with EXOSAT during a giant outburst in 1985 (Pamar et al. 1989a). In this system, the pulsar orbits a B0 Ve star (Motch & Janot-Pacheco 1987; Janot-Pacheco, Motch, & Pakull 1988; Coe et al. 1988) every 46 days (Wilson, Fabregat, & Coburn 2005). A normal outburst has been detected for nearly every periastron passage since 1991 (Wilson et al. 2002; Wilson, Fabregat, & Coburn 2005). For these normal outbursts, the outburst intensity and the global spin-up rate appeared to be tied to the K-band intensity of the Be star. From 1992-1994 EXO 2030+375's outbursts were bright and the pulsar was spinning-up. In 1994, shortly after a drop in the K-band intensity of the Be disk, the X-ray intensity abruptly dropped and the global trend changed to spin-down, indicating that the density of the Be disk had dropped and less material was available for accretion. The pulsar continued with faint X-ray outbursts and a global spin down trend until 2002, when again the K-band intensity increased to the 1992-1994 level followed by brighter X-ray outbursts and a transition to global spin-up (Wilson, Fabregat, & Coburn 2005). The outbursts continued to brighten and show spin-up until 2006 June when EXO 2030+375 underwent its first giant outburst since its discovery in

1985 (Corbet & Levine 2006; Krimm et al. 2006; McCollough et al. 2006; Wilson & Finger 2006). In this paper we present a timing analysis including twelve normal outbursts leading up to the giant outburst, the giant outburst, and seven normal outbursts after the giant outburst combined with previously published observations.

Accreting X-ray pulsars have strong surface magnetic fields of  $\sim 10^{12}$  G. A direct measurement of this field strength is provided by the energies of cyclotron resonance scattering features in their X-ray spectra. The magnetic field strength and the resonance energy are related as  $E_{\rm cyc}=11.6B_{12}(1+z)^{-1}$ , where  $B_{12}$  is the magnetic field strength in units of  $10^{12}$  G and z is the combined gravitational plus bulk motion Doppler shift (Nakajima et al. 2006, and references therein). The range of previously measured cyclotron features is from about 11 keV in 4U0115+63 Nakajima et al. (2006) to about 50 keV in A0535+262 (Terada et al. 2006). Previously a tentative cyclotron at 36 keV feature was reported in a 1996 normal outburst of EXO 2030+375 (Reig & Coe 1999); however, this feature has not been seen in other any other observations. Recent observations of EXO 2030+375 during its giant outburst have resulted in reports of a cyclotron feature near 10 keV (Wilson & Finger 2006; Klochkov et al. 2007). In this paper we present detailed spectral fits to RXTE observations from the giant outburst, demonstrating that the cyclotron feature was consistently detected over an extended period of time.

### 2. Observations and Analysis

Figure 1 shows the long-term flux history for EXO 2030+375 since its discovery as measured with EXOSAT, BATSE, and RXTE ASM. This Figure is provided here to aid the reader in placing the observations described below in context.

### 2.1. RXTE Observations

The 2006 giant outburst and five normal outbursts that followed from EXO 2030+375 were observed daily from 2006 June 22 through 2007 May 25 (MJD 53,908-54,245) with the Rossi X-ray Timing Explorer (RXTE) Proportional Counter Array (Jahoda et al. 2006, PCA) and the High-Energy X-ray Timing Experiment (Rothschild et al. 1998, HEXTE). Also included in this paper are analyses of previously unpublished RXTE observations of eight normal outbursts in the year prior to the giant outburst (MJD 53,540-53,868) and RXTE observations of outbursts in 2007 June (MJD 54,276-54,283) and 2007 August (MJD 54,322-54,329). For these outbursts, the typical 1-5 ks observations spanned about six days

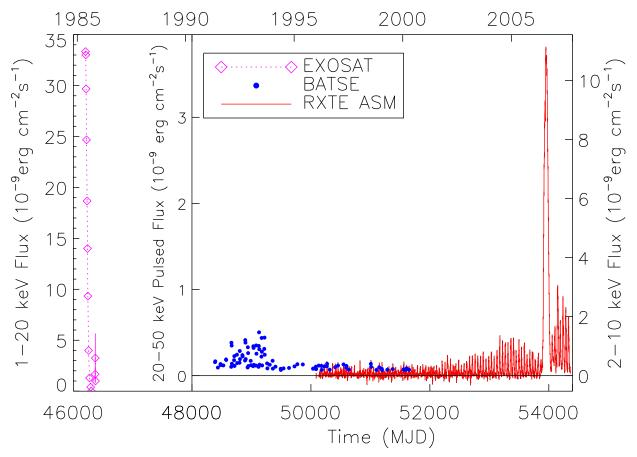


Fig. 1.— Long-term Flux history for EXO 2030+375. The pink diamonds and left y-axis denote EXOSAT 1-20 keV total flux measurements from Pamar et al. (1989a). Blue points and the y-axis near the center denote 20-50 keV pulsed fluxes measured with BATSE. Typically 1-4 of these BATSE points correspond to a normal outburst. The red histogram and right y-axis denote RXTE ASM 2-10 keV total flux measurements averaged over 4 days. Each spike corresponds to a normal outburst and the large peak is the 2006 giant outburst.

near the peak of the normal outburst. In this paper, timing analysis was performed using the Standard 1 PCA data, which has 0.125 s time resolution and no spectral resolution. Phase averaged spectral analysis was performed using the Standard 2 PCA data with 129 channel energy resolution and 16-s time resolution and the science data mode E\_8us\_256\_DX1F HEXTE data for cluster B only, since cluster A was not rocking and was not on-source during the early and late parts of the giant outburst.

### 2.2. INTEGRAL Observations

International Gamma Ray Astrophysics Laboratory (INTEGRAL) ISGRI (Ubertini et al. 2003) public data from revolutions 18-22 (MJD 52,615-52,627), 67 (MJD 52,661-52,662), 80 (MJD 52,800-52,802), 159-160 (MJD 53,036-53,041), and 185-193 (MJD 53,126-53,133) was also included in our timing analysis. Our software, described in detail for the revolutions 18-22 observations in Camero-Arranz et al. (2005), collected good events in the 20-60 keV band using the pixel information function when the source was in the partially or fully coded field-of view of ISGRI. The good events were then epoch folded using a simple phase model based on spin frequency measurements with RXTE and INTEGRAL. To avoid binning effects, each pulse profile was fit with a Fourier series of harmonic coefficients. A correction described in Camero-Arranz et al. (2005) was applied to account for aperiodic noise due to pulse profile variations and due to nearby noisy sources. A template profile was estimated from the average profile for revolutions 18-22. To generate phase offsets from the model, we then cross-correlated the individual profiles with the template profile. The new phases for each outburst were then fit with a linear or quadratic phase model and the process was repeated, creating new folded profiles, new harmonic coefficients, and new phase offsets. The pulse profiles were then combined over time to improve statistics and to allow the phase measurements to constrain spin-up during each outburst. Pulse phase measurements with INTEGRAL from five normal outbursts of EXO 2030+375 are used in this paper.

# 2.3. Timing Analysis

For each RXTE PCA observation, we generated a light curve file from Standard 1 data using FTOOLS v6.2. We corrected each light curve to one average PCU using the FTOOL correctle. Using faxbary we corrected the times on each bin to the solar system barycenter. Then we corrected the times for the pulsar's orbit using the orbital parameters from Wilson, Fabregat, & Coburn (2005). Lastly, we fit a pulse profile model consisting of a 6th order Fourier expansion in the pulse phase model plus a constant background term. For

outbursts before and after the giant outburst where we did not have daily coverage, the phase model initially consisted of a constant frequency and was iteratively improved to a quadratic phase model for each outburst. For the daily measurements, the model was a quadratic spline with each  $\sim$  5-day interval having an independent spin-up rate. To compensate for aperiodic noise due to pulse profile variations within each RXTE observation, we first subtracted the pulse profile model from the light curve and then computed a power spectrum. Within each power spectrum we computed the average noise power around each harmonic  $\bar{P}_n$  in the frequency range  $[(n-1/2)\nu, (n+1/2)\nu]$  where n is the harmonic number and  $\nu$  is the model frequency for that observation. The errors on the pulse profile harmonic coefficients were then inflated by  $(\bar{P}_n/2)^{(1/2)}$  where 2 is the assumed Poisson level. Phase offsets were computed by cross-correlating the individual profiles with a template profile.

Examination of the measured spin-up rates within the contiguous daily observations of the giant outburst and five normal outbursts showed a periodic dip in the spin-up rate, just before periastron, indicating that the orbital solution needed improvement. To improve the orbital solution, we combined our new phase measurements with previously published phase measurements from the Burst and Transient Source Experiment (BATSE) (Wilson et al. 2002, 51 outbursts: 1991-2000 (MJD 48,385-51,657)) RXTE (Wilson et al. 2002; Wilson, Fabregat, & Coburn 2005, 4 outbursts; 1996 (MJD 50,266-50,275), 1998 (MJD 50,821-50,828), 2002 (MJD 52,432-52,443), and 2003 (MJD 52,894-52,899)), and INTEGRAL (Camero-Arranz et al. 2005, 1 outburst; 2002). The phases were fit with a global orbital model plus a quadratic spline. Prior to the giant outburst and for outbursts from 2007 June through September, the quadratic spline had an independent frequency derivative for each outburst. Phase "slips", jumps in the pulse cycle count, were fit in large gaps between outbursts where no data were available to constrain the phase model. The large spin-up rates during the giant outburst overwhelmed the orbital effects, so it was excluded from orbital analysis.

We found, however, that our initial fits were much poorer than expected, with reduced  $\chi^2$  values of about 2.0. Neither the phase residuals nor the phase errors showed any dependence on intensity or orbital phase, suggesting that the phase errors were simply too small across the board, indicating that the phase errors did not sufficiently reflect the effects of pulse profile variations from observation to observation. We added a systematic error of  $2.4 \times 10^{-3}$  cycles in quadrature to all of the phase measurements included in our fits. In addition we eliminated six BATSE points that were large outliers despite the already large BATSE error bars.

Table 1 lists the orbital parameters resulting from our fits: the orbital period  $P_{\text{orb}}$ , the epoch of periastron passage  $T_{\text{peri}}$ , the projected semi-major axis  $x = a_x \sin i$ , the eccentricity

e, and the periapse angle  $\omega$ . The largest differences between our new orbital fit (Fit 1) and published results (Wilson, Fabregat, & Coburn 2005) are in e (2.9 $\sigma$  smaller) and  $a_x \sin i$  (2.5 $\sigma$  larger). Next we searched for time dependent variations in the orbital parameters, fitting the orbital period derivative  $\dot{P}_{\rm orb}$ , the derivative of the periapse angle  $\dot{\omega}$ , and the derivative of the projected semi-major axis  $\dot{x}$ . First we varied each parameter separately, holding the other two fixed at zero, while allowing all other fit parameters to vary. Varying  $\dot{\omega}$  produced the most significant result (Fit 2), with an F-test significance of 3.4 $\sigma$ .  $\dot{P}_{\rm orb}$  and  $\dot{x}$  were less significant with F-test values of 1.7 $\sigma$  and 3.0 $\sigma$ , respectively. Next we tried varying both  $\dot{\omega}$  and  $\dot{x}$  (Fit 3) while holding  $\dot{P}_{\rm orb}$  fixed at zero and allowing all other parameters to vary. This fit had an F-test significance of 3.6 $\sigma$  for two parameters and 2.0 $\sigma$  for the addition of  $\dot{x}$ . Lastly we tried varying all three parameters (Fit 4). This fit had an F-test significance of 3.7 $\sigma$  for the addition of three parameters and 2.0 $\sigma$  for just the addition of  $\dot{P}_{\rm orb}$ .

Figure 2 shows the phase residuals for all phase measurements after BATSE was deorbited in May 2000. Phase residuals prior to this date are shown in Wilson et al. (2002). Figure 3 zooms in to show the 2-60 keV rms pulsed flux overlaid with the frequency derivatives estimated from the orbit fitting and the phase residuals. From this figure, we note that the spin-up rate and pulsed flux are clearly correlated across all orbital phases. At the end of the giant outburst, the pulsar spins down briefly. The minimum in the frequency derivative precedes the pulsed flux minimum slightly. Although there are clearly defined outbursts for each orbit, the pulsed flux never drops to zero between outbursts and we see considerable flaring activity in the intra-outburst region.

Using the orbit from Fit 3 in Table 1, we fit the phase measurements for the giant outburst with a new quadratic spline model in which each 5-day interval had an independent frequency derivative. Figure 4 shows the spin frequency, the spin-up rate, and the 2-100 keV flux determined for the giant outburst. The giant outburst reached a peak spin-up rate of  $(1.815 \pm 0.006) \times 10^{-11}$  Hz s<sup>-1</sup> for the 5-day interval 2006 August 1-6 (MJD 53948-53953). The 2-100 keV flux also peaked in this interval at  $(3.59 \pm 0.07) \times 10^{-8}$  erg cm<sup>-2</sup> s<sup>-1</sup>.

# 2.4. X-ray Spectral Analysis

Data analysis was performed using FTOOLS v6.1.2 (Blackburn 1995)<sup>1</sup>. For each RXTE PCA observation, we created a background spectrum using the bright source model with the FTOOL pcabackest and extracted source and background spectra using the FTOOL

<sup>1</sup>http://heasarc.gsfc.nasa.gov/ftools/

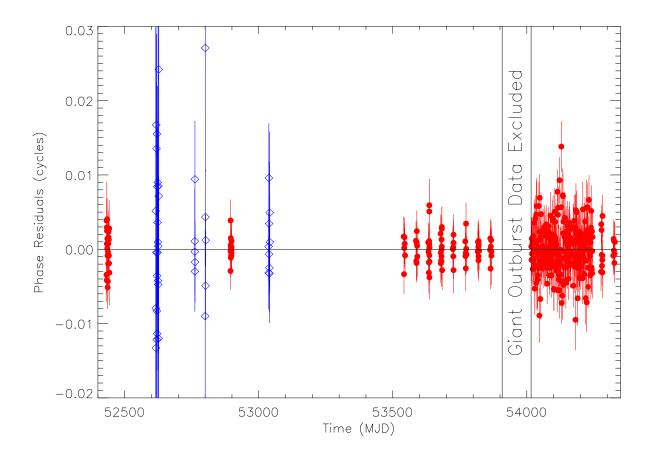


Fig. 2.— Phase residuals for all of the measurements after May 2000 included in the fitting. Red filled circles denote *RXTE* measurements and blue open diamonds denote *INTEGRAL* measurements. Phase residuals from BATSE and *RXTE* before May 2000 are shown in Wilson et al. (2002). The differences between this orbital fit and that one are too small to be visually apparent.

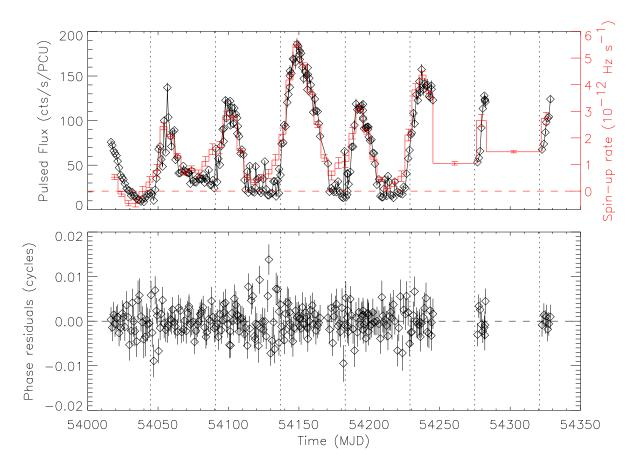


Fig. 3.— A close look at timing results after the giant outburst. *Top:* 2-60 keV rms pulsed flux measured with the *RXTE* PCA (left y-axis, black diamonds) overlaid with the estimated model frequency derivatives (right y-axis, red histogram). The red dashed line denotes a frequency derivative equal to zero. *Bottom:* Phase residuals after the giant outburst.

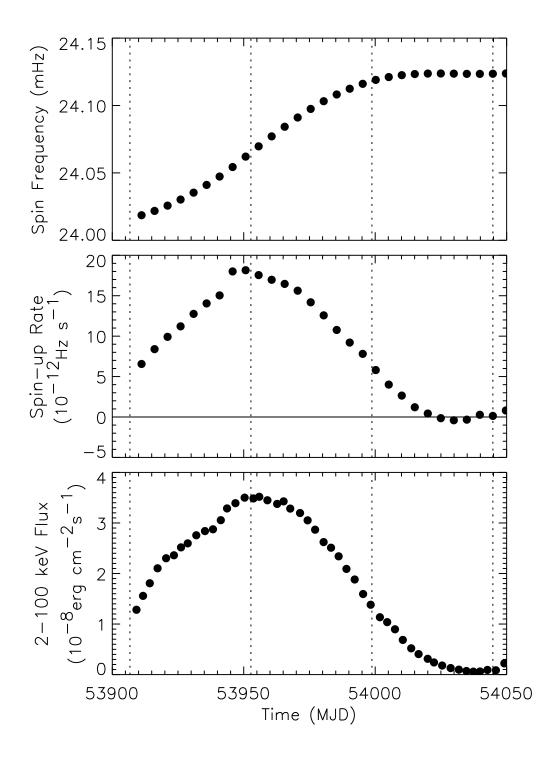


Fig. 4.— Measured spin-frequency, spin-up rate, and 2-100 keV flux for the 2006 giant outburst from RXTE data. Each frequency and spin-up rate point corresponds to the average barycentered, orbit corrected (using Fit 3), frequency and frequency derivative for a 5-day interval of RXTE PCA observations. The bottom panel shows 3-day averages of the total 2-100 keV flux measured with joint spectral fits to RXTE PCA and HEXTE data.

saextract. In addition we corrected for deadtime following the recipe <sup>2</sup>. A 0.5% systematic error was included. For HEXTE cluster B data, detectors 0,1, and 3, we separated the data into source and background using the FTOOL hxtback and extracted source and background spectra using seextrct. HEXTE spectra were corrected for deadtime using hxtdead. An analysis that includes HEXTE cluster A data is described in Camero-Arranz (2007). The results were consistent with ours. Unfortunately cluster A was not on-source during the early and late parts of the giant outburst, so the data set is more limited. Six observations (obsids 91089-01-01-04, 91089-01-02-10, 91890-01-03-10, 91089-01-04-02, 91089-01-12-01, 91089-01-15-04) were excluded from our analysis because they had less than 20 seconds of HEXTE cluster B background exposure, i.e. HEXTE cluster B was not rocking. Only the last two of these observations were during the giant outburst.

From a joint fit to RXTE PCA and HEXTE data from August 15, 2006 (MJD 53962), we found evidence for a cyclotron scattering feature near 10 keV (Wilson & Finger 2006). The model used was an absorbed power-law (PHABS\*POWERLAW) with a high-energy cut-off (HIGHECUT), an iron line (GAUSSIAN), and a Gaussian cyclotron absorption line (GABS). The power-law had a photon index of 1.53(2), with a cutoff energy at 12.4(4) keV, a folding energy of 27.4(5) keV. The cyclotron energy was 10.1(2) keV, with a Gaussian width of 3.3(2) keV and a peak depth of 1.1(1). This feature was significant at a 7.5 sigma level. Other continuum models, e.g., a Bremsstrahlung model, also showed evidence for this feature.

Using Xspec v12.3, we first fit the PCA and HEXTE data from each observation with an absorbed power-law with a high energy cutoff plus a Gaussian iron line (PHABS (POWER-LAW+GAUSSIAN) HIGHECUT). Based upon our previous detection of a cyclotron feature at 10 keV (Wilson & Finger 2006), we included a Gaussian absorption feature (GAUSS-ABS) to represent the cyclotron line. We discovered a problem with the built-in XSPEC model GABS. This model calls the Gaussian line model and then exponentiates it. However, the Gaussian line model returns the integral of the Gaussian across the input bins rather than the value of the Gaussian, resulting in GABS being incorrectly integrated. We wrote a local model GAUSSABS using the parameterization of Coburn et al. (2002). Figure 5 shows the spectrum and residuals with and without the Gaussian absorption feature for an observation on 2006 August 7 (MJD 53954.5) near the peak of the outburst. Dips are visible at 10 and 20 keV. Figure 6 shows the cyclotron feature parameters: the line energy E, the line width  $\sigma$ , and the optical depth  $\tau$  defined in Equations 6 and 7 in Coburn et al. (2002). Dotted lines across each panel show the average value for that parameter ( $\bar{E} = 11.44 \pm 0.02$ 

<sup>&</sup>lt;sup>2</sup>http://heasarc.gsfc.nasa.gov/docs/xte/recipes/cook\_book.html

keV,  $\bar{\sigma} = 3.08 \pm 0.02$  keV, and  $\bar{\tau} = 0.1263 \pm 0.0009$ ). The second from the bottom panel in Figure 6 shows the F-test probability for including the cyclotron feature. The bottom panel shows the 2-100 keV flux for each observation. Figure 7 shows the values for the absorption  $N_H$ , the power-law photon index, the cutoff energy  $E_{\rm cut}$ , and the folding energy  $E_{\rm fold}$ . The 2-100 keV flux is again shown in the bottom panel for comparison. Lastly, Figure 8 shows the iron line parameters, the line energy, width, and normalization. In addition, we also examined fits that included an additional Gaussian absorption feature at  $E_{\rm cut}$ , the MPLCUT model of Coburn et al. (2002). An F-test showed that this component was not significant. Lastly we tried adding a second Gaussian absorption feature around 20 keV. We attempted two approaches, one where the line energy was exactly twice that of the other feature and one where both line energies were free to vary independently. F-tests showed that including a second cyclotron feature (using either approach) did not significantly improve the fit. For a small number of spectra near the peak of the outburst, we also tried fitting a spectrum including a bump near 15 keV after Klochkov et al. (2007) instead of a Gaussian absorption feature. For all six spectra we fit with this model, it was a significantly poorer fit than the Gaussian absorption feature.

#### 3. Discussion

#### 3.1. Evidence for a Cyclotron Feature

The giant outburst of EXO 2030+375 began in early June 2006 and lasted until the end of October 2006. From our spectral fitting, we consistently detected a cyclotron feature at about 11 keV from 2006 June 22 (MJD 53908), when pointed PCA and HEXTE observations began, until 2006 September 26 (MJD 54004). From 2006 September 26 through 2006 October 2 (MJD 54010), we still detected the feature in about half of the observations. After 2006 October 2, we did not consistently detect the feature. This means that we consistently detected the feature at luminosities greater than about  $5 \times 10^{37}$  erg s<sup>-1</sup>.

As a consistency check, we examine the expected relationship between the magnetic field and the maximum spin up rate,  $\dot{\nu}$ , for EXO 2030+375.

$$\dot{\nu} = 2.61 \times 10^{-11} \text{Hz s}^{-1} k^{1/2} \alpha^{8/7} \beta^{6/7} \left(\frac{M_x}{1.4 M_{\odot}}\right)^{-3/7} I_{45}^{-1} R_6^{12/7} \left(\frac{d}{7.1 \text{ kpc}}\right)^{12/7}$$

$$\left(\frac{E_{\text{cyc}}}{11 \text{ keV}}\right)^{8/7} \left(\frac{F_{\text{peak}}}{3.5 \times 10^{-8} \text{ erg cm}^{-2} \text{s}^{-1}}\right)^{6/7}$$
(1)

where  $k \simeq 0.5-1.0$  is a multiplier of the equation for the disk inner edge;  $\alpha = (1.31 \times 0.621) = 0.890$  accounts for the redshift of the cyclotron line  $1 + z \simeq 1.31$  and the general relativistic

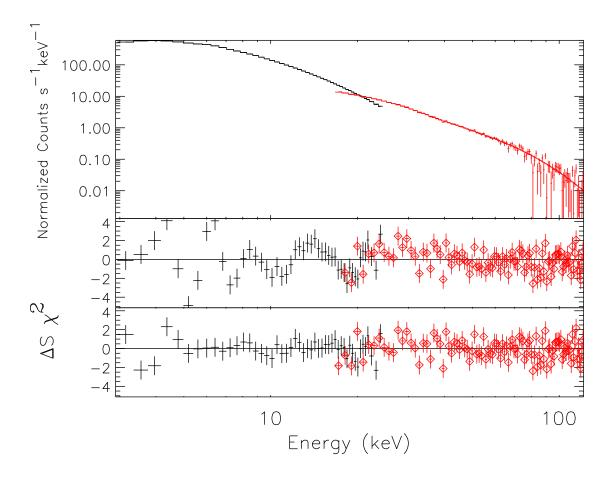


Fig. 5.— Energy spectra from 2007 August 7, near the peak of the outburst. In the top panel, the data were fit with a model consisting of an absorbed power law with a high energy cutoff with a Gaussian absorption feature representing the cyclotron feature and a Gaussian iron line. The center panel shows the residuals in units of sigmas for a fit that excluded the cyclotron feature. The bottom panel shows the residuals in units of sigmas with the cyclotron feature included in the model.

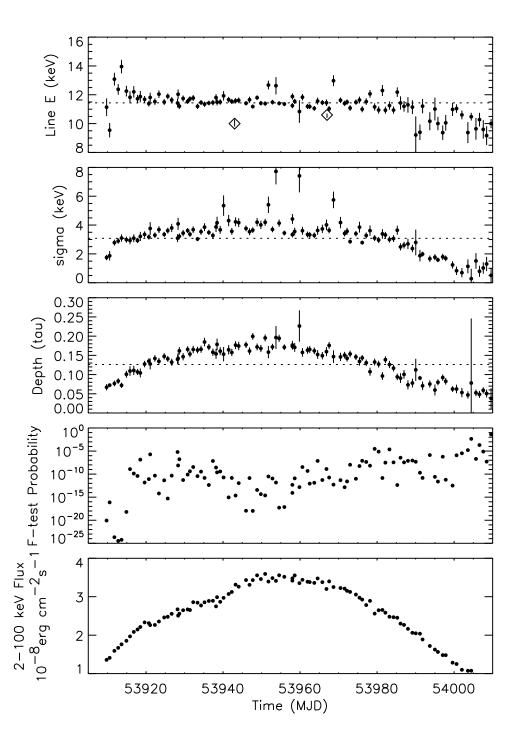


Fig. 6.— From top to bottom: EX0 2030+375 Cyclotron line energy (keV), width (keV), and optical depth defined in Equations 6 and 7 in Coburn et al. (2002). In the top panel, diamond symbols denote the line energy reported in Klochkov et al. (2007). Dotted lines show the average value for each parameter. The second from the bottom panel shows the F-test value in sigmas for including the cyclotron feature and the bottom panel shows the 2-100 keV flux.

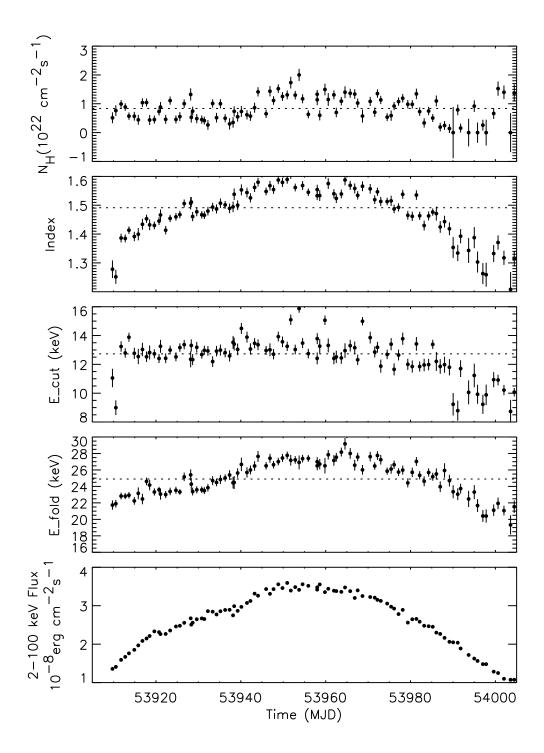


Fig. 7.— Additional model parameters, from top to bottom: the absorption  $N_{\rm H}$ , power-law photon index, Cut-off energy  $E_{\rm cut}$ , e-folding energy  $E_{\rm fold}$ , and the 2-100 keV flux.

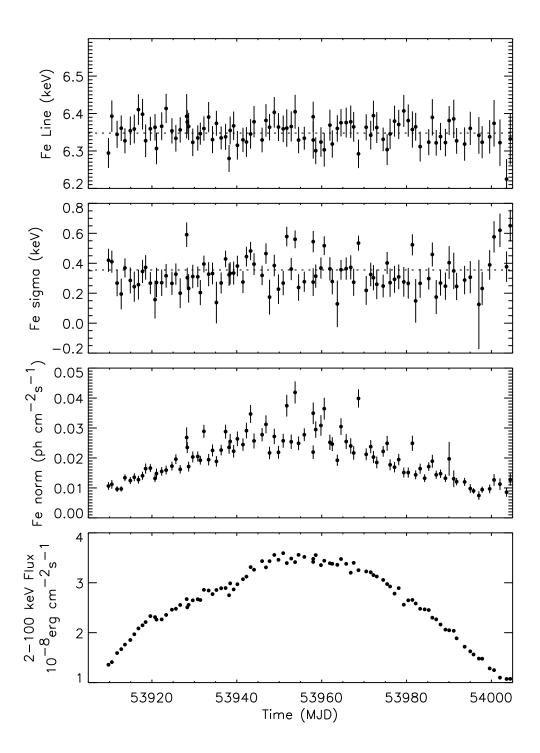


Fig. 8.— Gaussian Iron line model parameters, from top to bottom: the line energy (keV), line width (keV), the line normalization (photons  $cm^{-2} s^{-1}$ ), and the 2-100 keV Flux.

correction for the dipole field, 0.621 (See Wasserman & Shapiro 1983);  $\beta = L/4\pi d^2 F$  is the beaming factor, estimated to be 0.7-1.3, based on the range seen by eye in the pulse profiles (A more detailed study of the beaming factor based upon detailed modeling of pulse profiles is planned for a future paper.);  $M_x$  is the neutron star mass;  $I_{45}$  is the neutron star moment of inertia in units of  $10^{45}$  g cm<sup>2</sup>;  $R_6$  is the neutron star radius in units of  $10^6$  cm; d is the distance;  $E_{\rm cyc}$  is the cyclotron feature energy; and  $F_{\rm peak}$  is the peak flux. Our measured peak spin-up rate of  $1.815 \times 10^{11}$  Hz s<sup>-1</sup> is consistent with Equation 2 for  $k \simeq 0.5 - 0.9$ .

Examining Figure 6, we see that near the beginning of the outburst, the cyclotron line energy was smaller for the first two observations, 10-11 keV, then larger, about 13-14 keV. As the outburst brightened, the line energy evolved to about 11 keV, where it remained stable for much of the outburst. As the outburst began to fade, the cyclotron energy appeared to decrease; however, these observations were shorter than those taken at the beginning of the outburst, so the line parameters were less well-determined. The line depth and width also showed some possible luminosity dependence. In Figure 7, we see that the power-law photon index and the e-folding energy show evidence for a luminosity dependence. Lastly in Figure 8, only the Fe line normalization shows a luminosity dependence. This is expected for a Fe line that is due to EXO 2030+375 and not a background source.

INTEGRAL and Swift observations of EXO 2030+375 during the 2006 giant outburst revealed evidence for two cyclotron features at 10 and 20 keV (Klochkov et al. 2007). The lower energy feature lies slightly below our RXTE results. We believe this is related to problems with the GABS model in XSPEC discussed earlier. The 20 keV feature is not detected with RXTE. Other spectral parameters also differ between our RXTE measurements and INTEGRAL/Swift, likely due to inclusion of second line feature in the INTEGRAL/Swift spectrum and instrumental differences.

During an outburst in 1998, the Be/X-ray binary XTE J1946+274 was found to have cyclotron feature at about 35 keV (Heindl et al. 2001). The cyclotron feature appeared to have been consistently detected above  $3 \times 10^{-9}$  erg cm<sup>-2</sup> s<sup>-1</sup> (2-60 keV) corresponding to a luminosity of  $(2-4) \times 10^{37}$  erg s<sup>-1</sup> for an assumed distance of 8-10 kpc (Wilson et al. 2003), similar luminosities to where EXO 2030's feature was consistently detected. However, no evolution of the cyclotron feature with energy is seen in XTE J1946+274.

4U0115+63 observations with RXTE of an outburst in 1999 showed two cyclotron features at  $\sim 11$  and  $\sim 22$  keV for 3-50 keV luminosities of  $(5-13)\times 10^{37}$  erg s<sup>-1</sup>, assuming a distance of 7 kpc. As the luminosity decreased below  $\sim 5\times 10^{37}$  erg s<sup>-1</sup>, the second resonance disappeared and the fundamental resonance energy gradually increased, up to  $\sim 16$  keV at  $0.16\times 10^{37}$  erg s<sup>-1</sup> (Nakajima et al. 2006). Similar behavior was also observed in earlier outbursts. In 1990 February, two cyclotron features were detected at 11.3 and

22.1 keV, when the luminosity was  $1.4 \times 10^{38}$  erg s<sup>-1</sup>. In 1991 March, when the luminosity was  $2.0 \times 10^{37}$  erg s<sup>-1</sup>, the fundamental cyclotron feature was detected at 15.6 keV (Mihara, Makishima, & Nagase 2004). In both papers, the change in the cyclotron energy is believed to be related to a decrease in the height of the accretion shock in response to the reduction of the accretion rate; however, the existing models only qualitatively describe the observations. Above  $\sim 7 \times 10^{37}$  erg s<sup>-1</sup> the accretion shock height appears to saturate and is no longer correlated with luminosity (Nakajima et al. 2006). During the rise of its 2006 giant outburst, EXO 2030+375's cyclotron energy appears to saturate above about  $1.2 \times 10^{38}$  erg s<sup>-1</sup> (2-100 keV), assuming a distance of 7.1 kpc.

# 3.2. Long-Term Behavior

Figure 9 shows the long-term frequency history of EXO 2030+375 including measurements with EXOSAT (Pamar et al. 1989a), BATSE, INTEGRAL, and RXTE (Wilson et al. 2002; Wilson, Fabregat, & Coburn 2005). Figure 1 shows the long-term flux history, including EXOSAT measurements from Pamar et al. (1989a). Each spike in the ASM history corresponds to a normal outburst. Typically, 1-4 points in the BATSE history (Wilson et al. 2002) correspond to a normal outburst. The large peak is the 2006 giant outburst.

As of early September 2007, seven normal outbursts have been observed with RXTEfollowing the giant outburst. They continue to show considerable spin-up. During the first five of these outbursts, daily PCA observations detected EXO 2030+375 pulsations throughout its orbit. For the last two outbursts, PCA observations were taken only near the outburst peaks. Figure 1 shows that these outbursts are generally brighter than those just before the 2006 giant outburst. Further, the ASM observations continue to indicate that there is significant emission, even between the outbursts. Figure 10 shows the orbital phase of EXO 2030+375 outbursts since 1991. The points for the BATSE outbursts are taken from Wilson et al. (2002). The RXTE ASM data were divided into 46-day intervals and each interval was fit with a Gaussian to determine the outburst peak. Similarly, using a Gaussian fit to 120 days of ASM data, we found that the giant outburst peaked at 2.5 days after periastron, 1.9 orbits after the previous normal outburst. From 1991 to 1995, EXO 2030+375's outbursts consistently peaked about 6-days after periastron. At some point between 1993 and 1995, a precessing density perturbation developed in the Be star's disk. In late 1995, the density perturbation interacted with the neutron star's orbit at a phase corresponding to 2.5 days before perisastron. The outburst peaks then quickly migrated in orbital phase until late 1997 when the density perturbation lost contact with the neutron star's orbit at a phase corresponding to 2.5 days after periastron (Wilson et al.

Table 1. EXO 2030+375 Orbital Fits

Parameter	Fit 1	Fit 2	Fit 3	Fit 4
$P_{\text{orb}}$ (days)	$46.0205 \pm 0.0002$	$46.0213 \pm 0.0003$	$46.0211 \pm 0.0003$	$46.0207 \pm 0.0004$
$T_{ m peri}$	$54044.73 \pm 0.01$	$52756.17 \pm 0.01$	$52802.20 \pm 0.01$	$53308.45 \pm 0.02$
x (lt-s)	$244 \pm 2$	$246 \pm 2$	$248 \pm 2$	$248 \pm 2$
e	$0.412 \pm 0.001$	$0.410 \pm 0.001$	$0.409 \pm 0.001$	$0.410 \pm 0.01$
$\omega \text{ (deg)}$	$211.3 \pm 0.3$	$211.9 \pm 0.4$	$212.0 \pm 0.4$	$212.6 \pm 0.4$
$\dot{P}_{\rm orb}  ({\rm days/day})$				$(-4 \pm 2) \times 10^{-7}$
$\dot{\omega} \; (\mathrm{deg/year})$		$0.18 \pm 0.05$	$0.15 \pm 0.05$	$0.17 \pm 0.06$
$\dot{x}$ (lt-s/year)			$0.2 \pm 0.1$	$0.2 \pm 0.1$
$\chi^2/\mathrm{dof}$	689.8/656	677.5/655	673.4/654	669.4/653

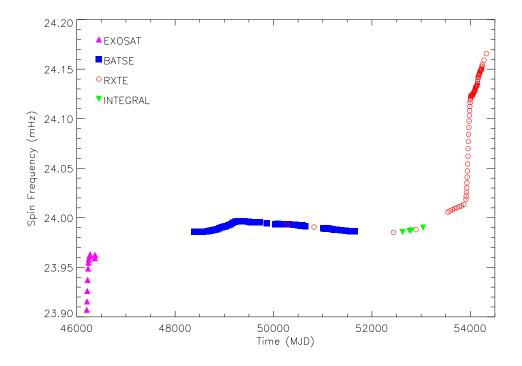


Fig. 9.— Barycentered, orbit corrected, spin-frequency measurements for EXO 2030+375 measured with EXOSAT, BATSE, RXTE PCA, and INTEGRAL.

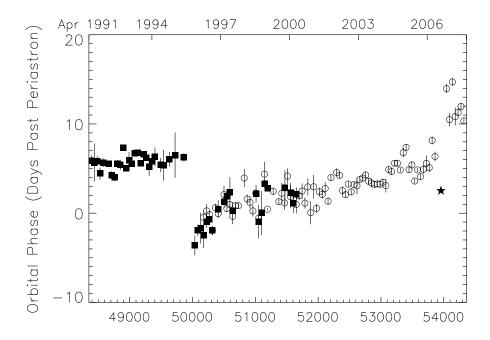


Fig. 10.— Orbital phase (in days past perisastron) of EXO 2030+375 outburst peaks. Normal outburst peaks measured with BATSE (squares) are taken from Wilson et al. (2002). Normal ( $open\ circles$ ) and giant (star) outburst peak orbital phases were determined from Gaussian fits to RXTE ASM data. The giant outburst peaked 1.9 orbits after the previous normal outburst peak.

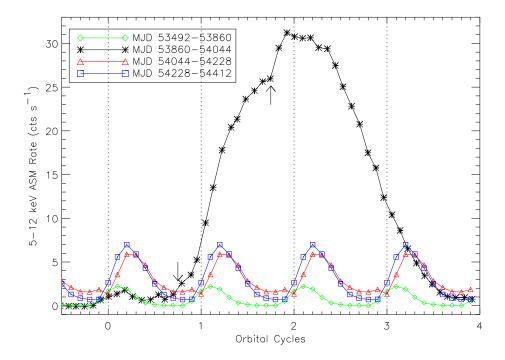


Fig. 11.— A comparison between the giant outburst and normal outbursts before and after it. The black line with asterisks denotes 4-day average RXTE ASM measurements in the 5-12 keV band for the giant outburst and its precursor normal outburst. Epoch-folded profiles, repeated 4.5 times, are shown for the eight outbursts preceding the giant outburst (denoted green diamonds), four outbursts immediately following the giant outburst (denoted by red triangles), and next three outbursts following those (denoted by blue squares). Arrows denote the approximate orbital phase of the initial rise of the giant outburst and the approximate orbital phase of an abrupt jump in flux. Both occur at orbital phase  $\sim 0.75$ .

2002; Wilson, Fabregat, & Coburn 2005). From 1997 until just before the giant outburst in 2006, the outburst orbital phases continued to slowly migrate. Just before the giant outburst in 2006, the outburst peaks had finally returned to approximately six days after periastron. After the giant outburst, the first normal outburst peaked at about 14 days after periastron as did the third and brightest of the normal outbursts. The remaining five normal outbursts peaked about 11 days after periastron. It is interesting to note that both sudden shifts in outburst phase are similar in magnitude, about 8-9 days, but opposite in sign.

Figure 11 shows a comparison between the giant outburst and the average profiles of normal outbursts before and after it. The giant outburst and the small normal outburst that preceded it are denoted by black asterisks. The normal outburst preceding the giant outburst was not particularly bright, occurred at the same orbital phase as the average profile for the preceding eight outbursts (green diamonds), but was unusual in that at about the point the outburst should have started fading, the flux remained higher than expected and then quickly rose into the giant outburst. Arrows on the plot denote orbital phase 0.75, where the giant outburst appears to be starting to rise rapidly, and where we see a rapid increase in flux one orbit later. The average profile from the first four outbursts following the giant outburst (red triangles) shows that those outbursts began later in orbital phase and had a higher intra-outburst flux than the pre-giant outbursts and the later post-giant outbursts (blue squares). From Figures 11 and 1, the intra-outburst flux is slowly fading. It appears to be a long-lived tail of the giant outburst. A long-lived tail of a giant outburst has not been observed before in Be/X-ray binaries.

From our orbital fits using 17 years of EXO 2030+375 data, we see marginal evidence for apsidal precession. Our measurements are consistent with predictions from simple calculations given below. In the supernova explosions that form Be X-ray binaries the neutron star will receive a kick out of the original orbital plane. If the orbit is misaligned with the companion's spin axis, precession of the orbital plane is expected. Using calculations described in Lai, Bildsten, & Kaspi (1995) we estimate the magnitude of the expected effect due to interactions between the companion's rotation period and the orbit. The apsidal motion and orbital plane precession change  $\omega$  the observed longitude of periastron and i the orbital inclination angle. Using Equation 7 in Lai, Bildsten, & Kaspi (1995) to calculate the apsidal rate  $\dot{\omega}$  gives

$$\dot{\omega} = 1.6 \times 10^{-3} \left( \frac{46.0208 \text{ days}}{P_{\text{orb}}} \right) \left( \frac{k}{0.01} \right) \left( \frac{8.9 R_{\text{c}} \sin i}{a_{\text{x}}} \right)^{2}$$

$$\times \left( \frac{\hat{\Omega}_{\text{s}}}{0.5} \right) \left( 1 - \frac{3}{2} \sin^{2} \theta \right) \text{ rad yr}^{-1}.$$

$$(2)$$

where  $k \simeq 0.01$  is the apsidal motion constant for a  $10M_{\odot}$  main-sequence star (Lai, Bildsten, & Kaspi

1995);  $R_{\rm c} = 6R_{\odot}$  is the assumed Be star radius;  $\hat{\Omega}_{\rm s}$  is the dimensionless spin of the companion, assumed to be near break-up  $\hat{\Omega}_{\rm s,max} = 0.5$ ;  $a_{\rm x}$  is the measured semi-major-axis;  $P_{\rm orb}$  is the measured orbital period (see Table 1); i is the orbital inclination angle; and  $\theta$  is the angle between the orbital angular momentum and the spin angular momentum.

From our orbital fits, we measured apsidal rates ranging from  $(2.6 \pm 0.9) \times 10^{-3}$  radians yr<sup>-1</sup> (Fit 3, Table 1) to  $(3.1 \pm 0.9) \times 10^{-3}$  radians yr<sup>-1</sup> (Fit 2, Table 1). Our measurements are within a factor of about 2 of the simple calculations, suggesting that we are seeing apsidal motion in this system. The change in i is given by Equation 8 in Lai, Bildsten, & Kaspi (1995) and has the same magnitude as  $\dot{\omega}$ 

$$\frac{\mathrm{d}i}{\mathrm{d}t} = 1.6 \times 10^{-3} \left(\frac{46.0208 \,\mathrm{days}}{P_{\mathrm{orb}}}\right) \left(\frac{k}{0.01}\right) \left(\frac{8.9R_{\mathrm{c}} \sin i}{a_{\mathrm{x}}}\right)^{2} \times \left(\frac{\hat{\Omega}_{\mathrm{s}}}{0.5}\right) \sin \theta \cos \theta \sin \Phi \,\mathrm{rad} \,\mathrm{yr}^{-1}.$$
(3)

In Fits 2 and 3, we see a suggestion of a change in i,  $di/dt = (0.8 \pm 0.4) \times 10^{-3} \, \text{sin}^{-1} \, i$  radians  $\text{yr}^{-1}$ , also consistent with the calculation within a factor of about two.

### 3.3. Comparison with 1985 Giant outburst

In the discovery outburst observed with EXOSAT in 1985, the maximum observed luminosity in the 1-20 keV band was  $2\times10^{38}~{\rm erg~cm^{-2}~s^{-1}}$  (Pamar et al. 1989a). The maximum 2-20 keV luminosity observed with RXTE PCA was  $1.44 \times 10^{38}$  erg cm<sup>-2</sup> s<sup>-1</sup>, about 72% of the EXOSAT value. Both luminosities assume a distance of 7.1 kpc (Wilson et al. 2002). The difference cannot be explained from absorption, suggesting that the 1985 outburst was brighter. Further evidence for this comes from comparing the peak spin-up rates from both outbursts. The peak spin-up rate measured in the 1985 outburst was  $2.4 \times 10^{-11}$  Hz s<sup>-1</sup>, while the peak spin-up rate measured in the 2006 outburst was  $(1.815 \pm 0.006) \times 10^{-11} \text{ Hz}$ s<sup>-1</sup>, also about 75% of the EXOSAT value. However, despite the fainter peak, the 2-20 flux minimum reached after the 2006 outburst was  $(4.0\pm0.4)\times10^{-10}~{\rm erg~cm^{-2}~s^{-1}}$  much brighter than the 1985 upper limit of  $1.3 \times 10^{-11}$  erg cm<sup>-2</sup> s<sup>-1</sup> (1-20 keV). The 2006 flux minimum occurred about 90 days after the peak and similarly the 1985 upper limit was measured 98 days after the initial and brightest detection. Presumably, the EXOSAT detections of EXO 2030+375 from 1985 October 29 - November 3 (Parmar, White, & Stella 1989) corresponded to a normal outburst. Using our best ephemeris, we find that these observations span orbital phases of 8.5 to 13.5 days past periastron, very similar to the orbital phases where we see normal outbursts after the 2006 giant outburst. The first normal outburst after the 2006 giant outburst reached a peak 2-20 keV flux of about  $6.6 \times 10^{-9}$  erg cm<sup>-2</sup> s<sup>-1</sup>, approximately a factor of two brighter than the non-flaring observation on 1985 November 3 and a factor of about 3 fainter than the brightest flares on 1985 October 30-31 (Parmar, White, & Stella 1989). From Figure 3 it is clear that considerable day to day variability was present especially in the first outburst after the 2006 giant outburst and between outbursts. This variability may be related to the flaring seen on 1985 October 30-31. Both flaring episodes occurred at similar orbital phases; however, our RXTE observations were too short to confirm if the same flaring behavior was occurring.

#### 4. Conclusions

EXO 2030+375 has now been observed for more than 22 years. In this time, it underwent two giant outbursts, in 1985 and 2006, and numerous normal outbursts. Weak evidence for evolution of the binary orbit is presented in this paper. Perhaps by the next giant outburst this can be accurately determined. In 2006, we observed the onset of a giant outburst of EXO 2030+375 for the first time. A normal outburst, which peaked slightly later than the previous ones, preceded the 2006 giant outburst. Near orbital phase 0.5 (See Figure 11) the flux from EXO 2030+375 began to increase instead of declining as it usually would after a normal outburst. The flux and spin-up rate continued to increase for more than an entire orbit. Near orbital phase 0.75, the flux abruptly increased, accompanied by an abrupt increase in the spin-up rate. This was followed by a relatively flat-topped maximum during which the flux remained within 10% of the maximum for about 25 days, from orbital phase -0.2 to 0.35. After that, the flux declined to a minimum more than 1.5 orbits later. The entire giant outburst spanned more than three pulsar orbits.

During the 2006 giant outburst, we discovered evidence for a cyclotron feature with a mean value of  $11.44 \pm 0.02$  keV that was consistently detected for about 90 days, at 2-100 keV luminosities above  $5 \times 10^{37}$  erg s<sup>-1</sup>. This feature translates into a magnetic field strength of  $B = 9.9 \times 10^{11} (1+z)$  G  $\simeq 1.3 \times 10^{12}$  G. Predictions of the peak spin-up rate during the giant outburst, using this magnetic field strength, are consistent with the measured peak spin-up rate during the 2006 giant outburst. Klochkov et al. (2007) proposed that the EXO 2030+375 spectrum measured with *INTEGRAL* and *Swift* could also be explained by a model containing a bump at 15 keV. However, our *RXTE* observations do not appear to support that model. The cyclotron features for EXO 2030+375 and 4U 0115+63 (Nakajima et al. 2006) have the lowest energies measured to date. Now we are left with the question: Is the lack of detections of  $E_{\rm cyc} < 10$  keV a physical or observational bias?

The two classes, normal (type I) and giant (type II), of Be/X-ray pulsar outbursts are

clearly distinguishable in the observations of EXO 2030+375. However, the evolution seen in the phasing, duration, and peak flux of the normal outbursts, while apparently related to the Be star's disk (Wilson et al. 2002), is poorly understood. The lack of gaps in detection between the normal outbursts after the 2006 giant outburst implies that the accretion disk present in the giant outburst persists throughout these normal outbursts. Many have believed that the giant outbursts and normal outbursts were distinguished by the presence of an accretion disk in the giant outburst, while the normal outbursts proceeded by wind accretion. Possibly the normal outbursts following a giant outburst (as in the "mother duck/baby duck" complexes seen with BATSE in Bildsten et al. 1997) are a distinct class of normal outbursts, with the remainder proceeding by wind accretion. However, XTE J1946+274 (Wilson et al. 2003) had a series of normal outbursts that also had no detection gaps between them, but these outbursts were not preceded by a giant outburst. Ikhsanov (2001) show for longer period sources, e.g. A0535+26, disk accretion is required for the normal outbursts to occur. Hayasaki & Okazaki (2004) conclude from simulations that a transient disk forms in normal outbursts in shorter period systems, e.g. 4U0115+63. Measurements of significant spin-up during normal outbursts of EXO 2030+375 prior to the 2006 giant outburst (Wilson et al. 2002; Wilson, Fabregat, & Coburn 2005) suggested that at least a transient accretion disk was also present in those outbursts. Further, Hayasaki & Okazaki (2006) conclude from simulations that accretion disks in Be/X-ray binaries evolve through three phases: a 'developing phase' where the mass accretion rate is double-peaked, but dominated by direct accretion at periastron; a 'transition phase' where the mass accretion rate evolves from double-peaked to single peaked as the approximately Keplerian disk grows with time; and finally a quasi-steady state where the mass accretion rate has a single peak induced by a one-armed spiral wave and is on average balanced with the mass-transfer rate from the Be disk. Camero-Arranz et al. (2005) reported multiple detections of an initial spike preceding the main peak in outbursts prior to the giant outburst. This initial spike was usually smaller than the main outburst peak, suggesting that EXO 2030+375 was in the 'transition phase.' After the giant outburst, the initial spike preceding the main peak has disappeared from the normal outbursts, suggesting that the accretion disk in EXO 2030+375 has reached the final quasi-steady state. Therefore, the long-term behavior seen in the normal outbursts of EXO 2030+375 appears to be product of the state of the Be disk and the accretion disk, allowing for a wide range of variations.

Giant outbursts from EXO 2030+375 also vary in brightness and in orbital phase. The 2006 giant outburst peaked at a 2-100 keV luminosity of  $2.2 \times 10^{38}$  erg s<sup>-1</sup>. In the 2006 giant outburst, the 2-20 keV luminosity and the peak spin-up rate were about 72% and 75%, respectively, of that measured in the the 1985 outburst, suggesting that the 1985 outburst had a 2-100 keV peak luminosity of  $(2.9-3.0)\times 10^{38}$  erg s<sup>-1</sup>, which was super-Eddington unless

the neutron star mass was greater than about  $2.2M_{\odot}$ . The 1985 outburst was shifted by 0.65 in orbital phase relative to the decline of the 2006 outburst. Interestingly, the decay constants of both outbursts were very similar. Giant outbursts in EXO 2030+375 do not appear to be locked in orbital phase, unless the onsets are. The 2006 minimum spanned orbital phase -0.2 to -0.1, very similar to the orbital phase of the 23 August 1985 minimum; however, the 2006 minimum was more than 30 times brighter than in 1985. Despite the differences between the giant outbursts, the normal outburst following the 1985 giant outburst lined up quite well in orbital phase with the second normal outburst following the 2006 giant outburst. Both normal outbursts also showed flaring activity.

This research has made use of data obtained from the High Energy Astrophysics Science Archive Research Center (HEASARC), provided by NASA's Goddard Space Flight Center (GSFC). RXTE ASM quick-look results were provided by the RXTE ASM teams at MIT and at the GSFC SOF and GOF. We thank Morgan Dwyer, a summer intern from Yale who performed the early timing analyses as the observations originally came in. We also thank Evan Smith and Jean Swank for their help scheduling the daily RXTE observations of the giant outburst and of the normal outbursts that followed.

#### REFERENCES

Arnaud, K.A. 1996, Astronomical Data Analysis Software and Systems V, eds. G. Jacoby and J. Barnes, ASP Conf. Series, Vol 101, 17

Bildsten, L. et al. 1997, ApJS, 113, 367

Blackburn, J.K. 1995, in ASP Conf. Ser., Vol. 77, Astronomical Data Analysis Software and Systems IV, ed. R.A. Shaw, H.E. Payne, and J.J.E. Haynes (San Francisco: ASP), 367

Camero-Arranz, A. et al. 2005, A&A, 441, 261

Camero-Arranz, A. 2007, Ph.D. Thesis, Universidad de Valencia

Coburn, W. et al. 2002, ApJ, 580, 394

Coe, M.J. et al. 1988, MNRAS, 232, 865.

Corbet, R.H.D. 1986, MNRAS, 220, 1047

Corbet, R.H.D. & Levine, A.M. 2006, Atel #843

Hanuschik, R.W. 1996, A&A, 308, 170

Hayasaki, K. & Okazaki 2004, MNRAS, 350, 971

Hayasaki, K. & Okazaki 2006, MNRAS, 372, 1140

Heindl, W.A. et al. 2001, ApJ, 563,L35

Ikhsanov, N.R. 2001, A&A, 372, 227

Jahoda, K., Markwardt, C. B., Radeva, Y., Rots, A. H., Stark, M. J., Swank, J. H., Strohmayer, T. E., & Zhang, W. 2006, ApJS, 163, 401

Janot-Pacheco, E., Motch, C., & Pakull, M.W. 1988, A&A, 202, 81.

Klochkov, D. et al. 2007, A&A, in press, astro-ph/0701791

Krimm, H. et al. 2006, Atel # 861

Lai, D., Bildsten, L., & Kaspi, V.M. 1995, ApJ, 452, 819

Levine, A. M., Bradt, H., Cui, W., Jernigan, J. G., Morgan, E. H., Remillard, R., Shirey, R. E., & Smith, D. A. 1996, ApJ, 469, L33

McCollough, M.L. et al. 2006, Atel # 868

Mihara, T., Makishima, K., & Nagase, F. 2004, ApJ, 610, 390

Miroshnichenko, A.S. et al. 2001, A&A, 377, 485

Motch, C. & Janot-Pacheco 1987, A&A, 182, L55.

Nakajima, M., Mihara, T., Makishima, K., & Niko, H. 2006, ApJ, 646, 1125

Negueruela, I. et al. 2001, A&A, 369, 117

Okazaki, A.T. & Negueruela, I. 2001, A&A, 377, 161

Parmar, A.N. et al. 1989, ApJ, 338, 358

Parmar, A.N., White, N.E., Stella, L, 1989, 338, 373

Porter, J.M., Rivinus, T. 2003, PASP 115, 1153

Porter, J.M. 1996, MNRAS, 280, L31

Quirrenbach, A. et al. 1997, ApJ479, 477

Reig, P. & Coe, M.J. 1999, MNRAS, 302, 700

Rothschild, R. E., et al. 1998, ApJ, 496, 538

Stella, L., White, N.E. & Rosner, R. 1986, ApJ, 308, 669

Terada, Y. et al. 2006, ApJ, 648, L139

Ubertini, P. et al. (2003), A&A, 411, 131

Wasserman, I. & Shapiro, S.L. 1983, ApJ, 265, 1036

Waters, L.B.F.M. & van Kerkwijk, M.H. 1989, A&A, 223, 196

Wilson, C.A. et al. 2002, ApJ, 570, 287.

Wilson, C.A., Finger, M.H., Coe, M.J., Negueruela, I. 2003, ApJ, 584, 996

Wilson, C.A., Fabregat, J. & Coburn, W.2005, ApJ, 620, L99

Wilson, C.A. & Finger, M.H. 2006, Atel#877.

This preprint was prepared with the AAS  $\text{LAT}_{E\!X}$  macros v5.2.